ORIGINAL ARTICLE

JBMR®

Extracellular Vesicles From Osteotropic Breast Cancer Cells Affect Bone Resident Cells

Alexander Loftus,[1] Alfredo Cappariello,[2] Christopher George,[1] Argia Ucci,[1] Kirsty Shefferd,[1] Alice Green,[1] Riccardo Paone,[1] Marco Ponzetti,[1] Simona Delle Monache,[1] Maurizio Muraca,[3] Anna Teti,[1] and Nadia Rucci[1]

[1]Department of Biotechnological and Applied Clinical Sciences, University of L'Aquila, L'Aquila, Italy
[2]Oncohematology Department, IRCCS Bambino Gesù Children's Hospital Research Laboratories, Rome, Italy
[3]Department of Women's and Children's Health, University of Padua, Padua, Italy

ABSTRACT

Extracellular vesicles (EVs) are emerging as mediators of a range of pathological processes, including cancer. However, their role in bone metastases has been poorly explored. We investigated EV-mediated effects of osteotropic breast cancer cells (MDA-MB-231) on bone resident cells and endothelial cells. Pretreatment of osteoblasts with conditioned medium (CM) of MDA-MB-231 (MDA) cells promoted pro-osteoclastogenic and pro-angiogenic effects by osteoblast EVs (OB-EVs), as well as an increase of RANKL-positive OB-EVs. Moreover, when treating osteoblasts with MDA-EVs, we observed a reduction of their number, metabolic activity, and alkaline phosphatase (Alp) activity. MDA-EVs also reduced transcription of *Cyclin D1* and of the osteoblast-differentiating genes, while enhancing the expression of the pro-osteoclastogenic factors *Rankl*, *Lcn2*, *Il1b*, and *Il6*. Interestingly, a cytokine array on CM from osteoblasts treated with MDA-EVs showed an increase of the cytokines CCL3, CXCL2, Reg3G, and VEGF, while OPG and WISP1 were downregulated. MDA-EVs contained mRNAs of genes involved in bone metabolism, as well as cytokines, including PDGF-BB, CCL3, CCL27, VEGF, and Angiopoietin 2. In line with this profile, MDA-EVs increased osteoclastogenesis and in vivo angiogenesis. Finally, intraperitoneal injection of MDA-EVs in mice revealed their ability to reach the bone microenvironment and be integrated by osteoblasts and osteoclasts. In conclusion, we showed a role for osteoblast-derived EVs and tumor cell–derived EVs in the deregulation of bone and endothelial cell physiology, thus fueling the vicious cycle induced by bone tumors. © 2019 American Society for Bone and Mineral Research.

KEY WORDS: TUMOR-INDUCED BONE DISEASE; CANCER; OSTEOCLASTS; CELLS OF BONE; OSTEOBLASTS; CELLS OF BONE; OTHER; CELL/TISSUE SIGNALING - PARACRINE PATHWAYS; CYTOKINES; CELL/TISSUE SIGNALING - ENDOCRINE PATHWAYS

Introduction

Bone metastasis is a frequent complication of advanced breast cancer, with up to 70% incidence.[1] Although patients with bone metastases present with better prognosis than those with visceral metastases,[2] they experience severe morbidity, due to bone pain, increased risk of fracture, and hypercalcemia, resulting in a poor quality of life.[2] Bone mass is maintained in the physiological range by the concerted action of two cell types: bone-depositing osteoblasts and bone-resorbing osteoclasts, in a series of tightly coordinated molecular events. Osteoblasts produce macrophage-colony stimulating factor (M-CSF) and receptor activator of NF-κB ligand (RANKL), which interact with the osteoclast-expressed receptors c-fms and RANK, respectively.[3,4] RANK activation results in generation of mature osteoclasts, which form acidified seals on the bone surface to dissolve the mineral matrix components and into which proteases are subsequently secreted to degrade the underlying organic matrix.[5] The resulting release of growth factors and cytokines from the bone matrix and from osteoclasts stimulates osteoblasts to depose new bone matrix, closing the bone remodeling cycle.[5]

In metastatic breast cancer, the balance of bone remodeling is tilted toward a state of exacerbated bone destruction, whereby cancer cells secrete factors enhancing bone resorption and employ the subsequently released cytokines as stimuli for bone colonization.[6] Importantly, premetastatic cancer cells can establish bone lesions prior to metastasis, which suggests that a premetastatic niche is educated by breast cancer cells through mechanisms that are only partially known.[7]

Extracellular vesicles (EVs) are becoming established mediators of metastasis in a range of cancers.[8] They are membrane-

Received in original form March 11, 2019; revised form October 4, 2019; accepted October 6, 2019. Accepted manuscript online October 14, 2019.
Address correspondence to: Nadia Rucci, PhD, Department of Biotechnological and Applied Clinical Sciences, Via Vetoio – Coppito 2, 67100 L'Aquila, Italy.
E-mail: rucci@univaq.it
Additional Supporting Information may be found in the online version of this article.
Journal of Bone and Mineral Research, Vol. 35, No. 2, February 2020, pp 396–412.
DOI: 10.1002/jbmr.3891

derived carriers of biomolecules exchanged by cells in vivo, which allow direct transfer of functionally active proteins and nucleic acids to modify the behavior of recipient cells.[9] Despite the growing evidence that EVs are central to the metastatic process, their role in bone metastases is still an open field, which deserves to be investigated more. Results obtained so far demonstrate the ability of tumor-derived EVs to influence behavior of bone cells toward a microenvironment favoring their homing. Indeed, recent evidence indicates that exosomes isolated from metastatic breast cancer cells shuttle different protein cargoes, allowing breast cancer cell dissemination towards specific metastatic sites.[10] These exosomes are enriched in proteins related to migration and invasion, compared to exosomes isolated from non-metastatic breast cancer cells.[10] Consistent with the ability of tumor cell–derived EVs to drive organotropism, Hashimoto and colleagues[11] found that hsa-miR-940 shuttled by prostate cancer EVs enhances human mesenchymal stem cell differentiation toward an osteoblastic phenotype by targeting *ARHGAP1* and *FAM134A*. Moreover, forced expression of hsa-miR-940 in the osteotropic breast cancer cell line MDA-MB-231 reverts its propensity to induce osteolytic lesions toward an osteosclerotic phenotype,[11] thus indicating that the phenotype of bone metastases is also influenced by EV-shuttled miRNAs. Finally, a recent paper showed that exosomal release of L-plastin by MDA-MB-231 cells promotes their ability to induce osteolytic bone metastases in mouse models.[12]

Our recent studies have demonstrated extensive EV-mediated crosstalk between cells in the bone microenvironment.[13] Given these findings and the accumulating evidence showing that cancer cells can communicate with distant cells via EVs, we evaluated the impact of breast cancer cell EVs on cells resident in the bone microenvironment, finding a broad spectrum of pro-angiogenic, pro-osteoclastogenic, and anti-osteoblastogenic molecular events. Our data suggest a crucial role for breast cancer cell–derived EVs in the premetastatic dysregulation of bone remodeling.

Materials and Methods

Materials

Dulbecco's modified minimum essential medium (DMEM), fetal bovine serum (FBS), penicillin, streptomycin, and trypsin were from GIBCO (Uxbridge, UK). Sterile plasticware was from Falcon Becton-Dickinson (Oxford, UK). The RNeasy Mini™ kit (cat#74104), the RT^2 First Strand Kit (cat# 330401), and the Human Osteoporosis RT^2 Profiler PCR Array (cat# PAHS-170Z) were purchased from Qiagen (Düsseldorf, Germany). SYBR Green reagent was from Bioline (Memphis, TN, USA). DreamTaq Green master mix was from Thermo Scientific (Waltham, MA, USA). The mouse XL Cytokine Array Kit (cat#ARY028) was purchased from R&D Systems (Minneapolis, MN, USA). The human cytokine array kit (cat# ab193656) was from Abcam (Cambridge, UK). The Matrigel Matrix (cat#354262) was purchased by Corning (Corning, NY, USA), the in vitro Angiogenesis Assay (cat#ECM625) was from Millipore (Burlington, MA, USA). Anti-CD31 antibody (cat#ab124432), human recombinant VEGF (hrVEGF; cat#ab9751), and the human cytokine antibody array membrane (cat#ab193656) were from Abcam (Cambridge, UK), anti-Annexin II antibody (cat#71-3400), and anti-RANKL antibody (cat#sc-7628) were from Santa Cruz Biotechnology Inc. (Santa Cruz, CA, USA). The phycoerythrin (PE)-conjugated anti-RANKL antibody (cat#560295) and the endothelial cell growth supplement (ECGS; cat#354006) were purchased from BD Biosciences (Franklin Lakes, NJ, USA). The allophycocyanin (APC) anti-human Cd254 (RANKL; cat#347508) was from Biolegend (San Diego, CA, USA). The chemiluminescence reagent kit was purchased from Thermo Scientific (Waltham, MA, USA). The 3-(4,5-dimethylthiazol-2-yl)-2,5-diphenyltetrazolium (MTT) bromide reduction assay and all other reagents were from Sigma-Aldrich (St. Louis, MO, USA).

Animals

All procedures involving animals and their care were conducted in conformity with national and international laws and policies (European Economic Community Council Directive 86/609, OJ L 358, 1, December 12, 1987; Italian Legislative Decree 4.03.2014 n.26, *Gazzetta Ufficiale della Repubblica Italiana* no. 61, March 4, 2014; National Institutes of Health guide for the Care and Use of Laboratory Animals, National Institutes of Health Publication no. 85-23, 1985) and the Animal Research: Reporting of in vivo Experiments (ARRIVE) guidelines. Animal procedures also received institutional approval by the Italian Ministry of Health (Approval N. 173/2016-PR). Mice used for osteoblasts and osteoclast primary cultures were male and female, 7-day-old WT CD1; mice for the Matrigel plug assay experiments were female, 8-week-old WT CD1; mice for the in vivo tissue targeting were 7-day-old male and female WT of the CD1 strain. Mice were purchased by Charles River (Milan, Italy) and were housed in the animal facility of the University of L'Aquila, Italy, at the following conditions: temperature: 20°C to 24°C; humidity: 60% ± 5%; dark/light cycle: 12/12 hours. They had access to food and water *ad libitum* and were fed a standard diet (Mucedola, Milan, Italy. Code: 4RF21) composed of 60.8% carbohydrates, 21% proteins, 3.45% fat, 6.8% fibers, 7.95% trace elements, and 12% humidity. For these studies, mice were littermates and were randomized via software. Analyses were conducted in double-blind. No adverse events were observed during the course of the experiment.

Cell lines

The human breast cancer cell lines MDA-MB-231 (MDA) and MCF7, and the mouse breast cancer cell line 4T1 were obtained from the American Tissue Culture Collection (ATCC, Rockville, MD, USA) and grown in DMEM supplemented with 10% FBS, 100 IU/mL penicillin, 100 µg/mL streptomycin, and 2mM L-glutamine.

Human umbilical vein endothelial cells (HUVECs) were purchased from Lonza (Basel, Switzerland) and cultured in endothelial cell growth medium (EGM)-2. All cells were grown in a humidified 95% air/5% CO_2 incubator at 37°C.

Osteoblast primary cultures

Calvariae from 7-day-old WT CD1 mice were explanted, cleaned free of soft tissues, and digested three times with 1 mg/mL *Clostridium histolyticum* type IV collagenase and 0.25% trypsin, for 20 min at 37°C, with gentle agitation. Cells from the second and third digestions were plated following centrifugation at 200*g* for 7 min and grown in DMEM plus 10% FBS. At confluence, cells were trypsinized and plated according to the experimental protocol. The purity of the culture was evaluated by the transcriptional expression of the osteoblast markers alkaline phosphatase (Alp), Runt-related transcription factor 2 (Runx2), type I collagen, and osteocalcin and by the cytochemical evaluation of Alp activity.[14]

Alp activity assay

Primary mouse osteoblasts were fixed in 4% of buffered paraformaldehyde (PFA) for 15 min and washed twice with PBS. Alp activity was evaluated cytochemically by the Sigma-Aldrich kit n.85 L1, according to the manufacturer's instruction.

Osteoclast primary cultures

Femurs and tibiae of 7-day-old WT CD1 mice were cleaned of soft tissues, chopped with a sterile blade, and bone marrow was collected, diluted 1:1 in Hank's balanced salt solution (HBSS), layered over Histopaque 1077 solution, and centrifuged at 400*g* for 30 min. Buffy coat cells were collected, washed twice with HBSS, resuspended in DMEM plus 10% FBS, and plated in culture dishes at a density of 1×10^6 cells/cm^2. After 3 hours, cultures were washed with PBS to remove nonadherent cells and maintained for 7 days in the same medium supplemented with 50 ng/mL human recombinant M-CSF (hrM-CSF) and 120 ng/mL human recombinant RANKL (hrRANKL) as positive control or with M-CSF alone as negative control.[15] According to the experimental protocol, cells were also treated with EVs derived from osteoblasts and tumor cells for the timeframe of the culture, with or without suboptimal concentrations of hrRANKL (30 ng/mL). Committed precursors and mature osteoclasts were detected by histochemical staining of tartrate resistant acid phosphatase (TRAcP) activity (Sigma-Aldrich; cat#387A) according to the manufacturer's instructions.

EV isolation

EVs were isolated according to Cappariello and colleagues[13] and Kruger and colleagues.[16] Briefly, upon reaching 70% to 80% confluence, cells (osteoblasts, MDA-MB-231, MCF7, and 4T1) were washed in PBS and starved in serum-free DMEM to prevent contamination from FBS EVs. After 24 hours, culture medium was harvested and sequentially centrifuged at 300*g*, 4°C for 5 min to eliminate dead cells and at 5000*g*, 4°C for 25 min to eliminate membrane debris. Then, the supernatant was transferred to a Beckman L7-65 ultracentrifuge in a Beckman SW41-Ti rotor (both from Beckman Coulter, Indianapolis, IN, USA) and centrifuged at 100,000*g*, at 9°C for 70 min. Ultracentrifugation supernatant was discarded while the pellet, containing EVs, was resuspended in PBS, TRIzol, or radioimmunoprecipitation assay (RIPA) buffer according to the experimental protocol.

Transmission electron microscopy

Five microliters (5 μL) of EVs isolated from MDA-MB-231 CM (12 mL collected from one 175-cm^2 flask, cell density = 6.5×10^4 cells/cm^2) were put onto Formvar-coated grids and allowed to air dry. Grids were washed in PBS and fixed in 1% glutaraldehyde for 5 min. Samples were washed in distilled water and contrasted with 4% uranyl-oxalate solution for 5 min. Finally, grids were air dried for 10 min and observed under a Philips CM 30 transmission electron microscopy (TEM) at 80 kV.

RT^2 profiler real-time PCR array

RNA was isolated from MDA cells and from MDA-derived EV (MDA-EVs) using the RNeasy Mini™ kit (Qiagen), then RNA was reverse-transcribed employing the RT^2 First Strand Kit (Qiagen), according to the manufacturer's instructions. For MDA-EVs, 0.1 μg of RNA were subjected to a preamplification step using the PreAmp cDNA Synthesis Primer mix (Qiagen). cDNAs (from MDA cells or from MDA-EVs) were then mixed with RT^2 SYBR Green qPCR master mix and dispensed in the wells of the human osteoporosis PCR array. Wells were subjected to real-time PCR (Stratagene MX 3000), following the manufacturer's instructions. Array data were automatically analyzed by the dedicated software, RT^2 Profiler PCR Array data analysis template v3.2 (SuperArray Bioscience, Frederick, MD, USA). Briefly, after the fluorescence signal was collected and the threshold cycles (Cts) calculated by the machine, the average Ct of all genes was used as normalizer (ie, set to 1) to evaluate which genes were more or less expressed compared to the average Ct and plotted as such.

Comparative real-time RT-PCR

RNA was extracted using TRIzol reagent, then 1 μg of RNA was reverse-transcribed into cDNA using the Moloney Murine Leukemia Virus (M-MLV) reverse transcriptase and subjected to real-time RT-PCR (Roche LightCycler 96; Roche Diagnostics, Mannheim, Germany) using the primer pairs and amplification conditions described in Supplementary Table 1. All reactions were carried out using a SYBR green–based master mix containing ROX as reference dye. Data analyses were carried out via dedicated software (Roche LightCycler 96 software).

Endpoint RT-PCR

RNA was extracted using TRIzol reagent, then 1 μg was reverse transcribed using the M-MLV reverse transcriptase and subjected to PCR amplification with the DreamTaq Green master mix using the primer pairs and amplification conditions described in Supplementary Table 2. The PCR products were run in a 2% agarose gel with ethidium bromide.

Cytokine profiler arrays

For the mouse cytokine array profiling, 1 mL of conditioned medium (CM) collected from osteoblasts untreated or treated with MDA-EVs (isolated from 12 mL of CM collected from one 175-cm^2 flask, cell density = 6.5×10^4/cm^2) were added to the nitrocellulose membranes of the Mouse XL Cytokine Array Kit, which includes 111 capture antibodies printed in duplicate. The membranes were incubated overnight at 4°C, washed three times, and incubated with the detection antibody cocktail for 1 hour at room temperature (RT). After three washes, a 30-min incubation with the streptavidin–horseradish peroxidase (HRP) solution was performed, then membranes were washed and incubated with the Chemi Reagent mix for the detection of the positive spots by chemiluminescence. For data analysis, an Image J software (NIH, Bethesda, MD, USA; https://imagej.nih.gov/ij/) extension (protein array analysis) was used for the analysis. The intensity of each spot was determined by densitometry, and the average background subtracted. The normalization of the protein was performed by calculating the ratio between the signal intensity of the protein of interest and of the housekeeping proteins. For cytokine array analyses on EVs, the procedure was the similar, but EVs from 10 mL of medium were collected and lysed. Images were subjected to a despeckle algorithm (the ImageJ standard one) and contrast enhancement to improve the quality of the image.

For the human cytokine array, MDA-EVs were isolated from 120 mL of CM collected from ten 175-cm^2 flasks (cell density = 6.5×10^4/cm^2), then the pellet was resuspended in RIPA buffer

containing phosphatase and protease inhibitors and lysed by three cycles of freezing and thawing. Fifteen micrograms (15 μg) of proteins extracted from MDA-EVs were added to two separate nitrocellulose membranes after blocking. The membranes contain a total of 120 capture antibodies printed in duplicate, plus positive and negative controls/blanks. Membranes were incubated overnight at 4°C with the protein lysates, washed, and incubated for 2 hours at RT with the biotinylated detection antibody mix. After washing, membranes were incubated overnight at 4°C with streptavidin-HRP, washed, and the bioluminescence signal was detected as described for the human cytokine array. After background subtraction, signal was normalized by the average signal intensity, to evaluate which proteins were expressed above or below average.

Western blot analysis

For protein extraction, PC3 cells, MDA cells, MDA-EVs, and MCF7-EVs were lysed in RIPA buffer containing phosphatase and protease inhibitors. Fifty micrograms (50 μg) of protein cell lysates and 5 μg of EV protein lysate were resolved by 12% SDS-PAGE under reducing conditions and transferred to nitrocellulose membranes. Blots were probed with the primary antibody for 1 hour at RT, washed, and incubated with the appropriate HRP-conjugated secondary antibody for 1 hour at RT. Protein bands were visualized with the chemiluminescence reaction kit, according to the manufacturer's instructions and imaged on a Bio-Rad ChemiDoc XR Gel Imaging System (Bio-Rad Laboratories, Hercules, CA, USA).

Fluorescence-activated cell sorting of EVs

Fluorescence-activated cell sorting (FACS) analysis was performed on both osteoblast-EVs and MDA-EVs. Mouse primary osteoblasts were starved overnight in DMEM and treated with DMEM as control or with MDA- or 4T1-CM for 48 hours. Osteoblasts and MDA cells were washed three times with PBS, incubated for 24 hours with DMEM without serum before CM collection (12 mL, collected from one 175-cm^2 flask; cell density $3.5 \times 10^4/cm^2$ for osteoblasts and $6.5 \times 10^4/cm^2$ for MDA cells) and EV isolation. EV pellets were loaded with the membrane-permeant dye 5-chloro-methyl-fluorescein diacetate (CMFDA) for 30 min at 37°C, then incubated with a PE-conjugated anti-RANKL antibody (for OB-EVs) or with APC-conjugated RANKL antibody (for MDA-EVs) for 30 min at 4°C and analyzed on a BD FACSCANTO II (BD Biosciences). Nano-fluorescent standard particles (Spherotech, Lake Forest, IL, USA; cat#NFPPS-52-4 K) were used to set a dimensional gate up to 1 μm.

Cell viability assay

Viability of HUVECs and osteoblasts was assessed by the MTT bromide reduction assay following the manufacturer's protocol.

In vitro tube formation assay

The tube formation assay was carried out according to Kubota and colleagues.[17] Fifteen-well μ-Slides (Ibidi GmbH, Gräfelfing, Germany) were coated with Matrigel and allowed to solidify at 37°C for 30 min. HUVECs (1.5×10^4/well) were then plated and incubated with medium containing the following EVs: osteoblast EVs (OB-EVs), osteoblast EVs pretreated with MDA-CM (MDA_{CM}-OB-EVs), MDA-EVs, OB-EVs pretreated with MCF7-CM ($MCF7_{CM}$-OB-EVs), and MCF7-EVs. Each type of EV was isolated from 6 mL of CM collected from one Petri dish (75 cm^2; cell density: $3.5 \times 10^4/cm^2$ for osteoblasts, $6.5 \times 10^4/cm^2$ for MDA, and $4.5 \times 10^4/cm^2$ for MCF7). As positive control, HUVECs were treated with EGM-2. After 16 hours tube formation was inspected under an inverted light microscope at magnification 40×. Pictures were taken, and the percentage of branching points/area was evaluated (Branching Index) using an Image J extension system for angiogenesis analysis.

Matrigel plug assay

Eight-week-old male CD1 mice were subcutaneously injected in the ventral area with 0.4 mL Matrigel Matrix with 0.1 mL PBS (Neg.Ctrl), 0.1 mL of EVs isolated from MDA-CM (MDA-EVs), osteoblasts (OB-EVs), osteoblasts pretreated with MDA-CM (MDA_{CM}-OB-EVs), or with 0.1 mL containing endothelial cell growth supplement (ECGS) plus 150 ng/mL hrVEGF as positive control. Each mouse was injected with the number of EVs isolated from 12 mL of CM collected from one 175-cm^2 flask (cell density: $3.5 \times 10^4/cm^2$ for osteoblasts and $6.5 \times 10^4/cm^2$ for MDA). After 10 days mice were euthanized, and the plugs were removed, fixed in 4% buffered PFA, and processed for histology. No adverse effect or signs of animal distress were noted before euthanasia.

Excised Matrigel plugs were fixed in 4% buffered PFA and embedded in paraffin. Sections were cut using a Leica RM2125RT microtome (Leica, Wetzlar, Germany). Slide-mounted tissue sections (4 μm thick) were deparaffinized in xylene, hydrated serially in 100%, 95%, and 80% ethanol, and stained with hematoxylin/eosin. For immunohistochemistry, sections were deparaffinized, incubated with 0.07M citrate buffer (pH 6), 15 min at 98°C for antigen retrieval and treated with 3% H_2O_2 in PBS for 1 hour to quench endogenous peroxidases. Sections were then incubated with anti-CD31 primary antibody for 1 hour at RT. Finally, after washing, antibody binding was visualized using the Dako EnVision Detection kit (DAKO, Carpinteria, CA, USA) and 3,3′-Diaminobenzidine (DAB).

Mouse calvariae organ culture

Ex vivo osteolysis was assessed in mouse calvarial bone using an adaptation of the mouse calvarial organ culture.[18] Seven-day-old mice were euthanized, then calvariae were explanted, cleaned of soft tissues, and cultured in exosome-free DMEM plus FBS 10% with or without MDA-EVs isolated from 12 mL of CM collected from one 175-cm^2 flask (cell density $6.5 \times 10^4/cm^2$, number of mice/group = 3). Organ cultures were maintained for 7 days, the medium was changed twice, then calvariae were fixed in 4% buffered PFA and subjected to microCT (μCT) analysis.

μCT analysis

Calvaria images were acquired in a SkyScan 1174 μCT scanner (Bruker, Kontich, Belgium), with a pixel size of 6.7 μm (X-ray voltage 50 kV). The Skyscan Nrecon software was used for image reconstruction by employing a modified Feldkamp algorithm. Beam hardening correction and Fourier transform–based ring artifact reduction were applied to the reconstructed images. Area of the bone fraction was calculated for the calvarial bone–selected regions of interest using Image J software.

In vivo tumor EV targeting to bone

Seven-day-old CD1 mice were injected i.p. with fluorescent dye PKH26-labeled EVs isolated from MDA-CM (12 mL collected from one 175-cm^2 flask, cell density 6.5 × 10^4/cm^{2}injected to each mouse) or with PBS as control (number of mice/group = 9). After 5 hours, mice were euthanized, and bones were explanted and processed for lipidic extraction in chloroform-methanol (2:1 vol/-vol) and 0.125% wt/vol SDS. The lipophilic PKH26 fluorescence intensity was measured by spectrofluorometry (excitation wavelength 550 nm; emission wavelength 567 nm) in the extracted lipid fraction.

Explanted femurs and tibiae were flushed out to harvest bone marrow (BM) cells, which were fixed in 4% buffered PFA and run on a FACS Melody (BD Biosciences). Cell population was verified for PKH26 content (PE laser channel). After analysis, the PE-positive population was harvested on polylysine-coated glass slides automatically by the instrument. Slides were then mounted with a slow-fade, DAPI-containing mounting medium and evaluated by epifluorescence (Axioscope; Carl Zeiss Microscopy GmbH, Jena, Germany).

Femurs were also fixed in 4% buffered PFA and decalcified in 10% EDTA for 10 days. After cryopreservation in sucrose, bones were cryoembedded in optimal cutting temperature (OCT) compound in liquid nitrogen–cooled isopentane and cut to obtain 7-µm cryosections, which were washed in PBS to remove OCT, mounted, and evaluated by confocal microscopy (Leica TCS SP5 II; Leica).

For TRAcP activity evaluation, similarly obtained slides were hydrated and imaged by conventional epifluorescence for PKH26 (tetramethylrhodamine [TRITC] filter). Then, slides were unmounted and processed for TRAcP activity by histochemistry, according to the manufacturer's instructions (Sigma Aldrich; cat#387A), mounted with DAPI, and imaged by light microscopy and epifluorescence, respectively. It should be noted that epifluorescence is not able to resolve single EVs in our experimental conditions, hence the diffused appearance of the signal in epifluorescence images.

Results

Breast cancer–derived CM affects osteoblast differentiation

We first investigated the influence of the CM collected from the triple-negative and highly osteotropic human breast cancer cell line MDA-MB-231 (from now MDA) on osteoblasts. This treatment did not affect osteoblast metabolic activity evaluated by MTT test (Supplementary Fig. 1*A*), although reducing their number, evaluated by crystal violet staining (Supplementary Fig. 1*B*), as well as Alp activity (Supplementary Fig. 1*C*), thus indicating the ability of MDA-CM to impair osteoblast differentiation. In agreement with these results, MDA-CM reduced *Cyclin D1* mRNA, as well as the transcription of genes related to osteoblast differentiation *Alp*, *Runt-related transcription factor* (*Runx*)*2*, *Osterix* (*Osx*), *Bglap*, the gene coding for the late osteoblast differentiation marker osteocalcin, and the osteoblast function marker *Collagen 1a1* (*Col1a1*), compared to untreated osteoblasts (Supplementary Fig. 1*D*). Moreover, MDA-CM significantly increased mRNA expression of *Rankl*, whereas the Rankl decoy receptor *Osteoprotegerin* (*Opg*) and *M-csf* were not affected (Supplementary Fig. 1*E*). Treatment with MDA-CM also increased the transcriptional expression of the inflammatory and osteoclastogenic cytokines *Interleukin* (*Il*)*1b* and *Il6*, and of *Lipocalin 2* (*Lcn2*), the latter known to have a pro-tumoral effect and to inhibit osteoblast differentiation[19,20] (Supplementary Fig. 1*F*). Moreover, we found a significant increase of *Nitric oxide synthase 2* (*Nos2*) and a trend of increase of *Vascular endothelial growth factor* (*Vegf*) mRNAs in osteoblasts treated with MDA-CM (Supplementary Fig. 1*F*). ELISA on osteoblast CM confirmed the increase of RANKL, IL6, and Lcn2, whereas a trend of increase in IL1β secretion was observed (Supplementary Fig. 1*G*). Similar results were found in osteoblasts treated with CM harvested from the metastatic mouse breast cancer cell line 4T1 (Supplementary Fig. 2*A*–*D*), thus indicating that the molecular players are likely conserved from mice to human.

Considering the prominent role of RANKL in bone physiopathology and starting from our previous results showing that osteoblasts release RANKL-positive EVs,[13] we asked whether tumor cell CM could impact on this phenomenon. OB-EVs, isolated from untreated osteoblasts (Supplementary Fig. 3*A*) or osteoblasts treated with MDA-CM and 4T1-CM, were subjected to FACS analysis, which revealed a significant increase of the percent age of RANKL-positive EVs compared to EVs from untreated osteoblasts (Supplementary Fig. 3*B*,*C*).

Finally, we evaluated the effect of CM isolated from the less aggressive, epithelial-like, and estrogen receptor (ER)-positive human breast cancer cell line MCF7, finding no effect on either cell viability or cell number (Supplementary Fig. 4*A*,*B*), although a trend of reduction of Alp activity ($p = 0.06$) was observed compared to untreated osteoblasts (Supplementary Fig. 4*C*). However, a significant decrease of mRNA expression of osteoblast differentiation genes (Supplementary Fig. 4*D*) along with an increase of *Rankl* (Supplementary Fig. 4*E*) and of inflammatory cytokines was observed in osteoblasts treated with MCF7-CM (Supplementary Fig. 4*F*,*G*).

Taken together, this data shows the ability of tumor cell–released factors to influence the osteoblast transcriptional profile towards a less differentiated phenotype and to increase osteoblast production of pro-osteoclastogenic and inflammatory cytokines.

Characterization of MDA-derived EVs

We next asked whether the alterations in osteoblast behavior were mediated by breast cancer cell–derived EVs. We isolated EVs from breast cancer cell CM after 24 hours of conditioning under starvation. Size and concentration determination were performed by NanoSight (Salisbury, UK) (Supplementary Fig. 5*A*); Western blot analysis on protein extracts revealed positivity for Annexin II, one of the markers of EVs[21] (Supplementary Fig. 5*B*,*C*). The vesicular nature of the particles was confirmed by TEM, which showed membrane integrity and confirmed the expected EV size distribution of the MDA-EVs (Supplementary Fig. 5*D*).

We then characterized the transcriptional profile of MDA-EVs to assess whether mRNAs involved in the regulation of bone metabolism were present. RNA from MDA-EVs was extracted, reverse transcribed, and subjected to the osteoporosis real-time array, which includes 84 genes involved in bone remodeling. Among these genes, seven met the quality controls and cutoffs determined by our analyses (Fig. 1*A*). We confirmed, by semi-quantitative RT-PCR (Fig. 1*B*), that MDA-EVs shuttle mRNAs of key factors involved in osteoclast functions, such as *CLCN7*, encoding for the homodimeric chloride/proton antiporter ClC7, crucial for charge balance in the Howship lacuna, Integrin β_3 (*ITGB3*) and *CD40*, involved in osteoclast adhesion and

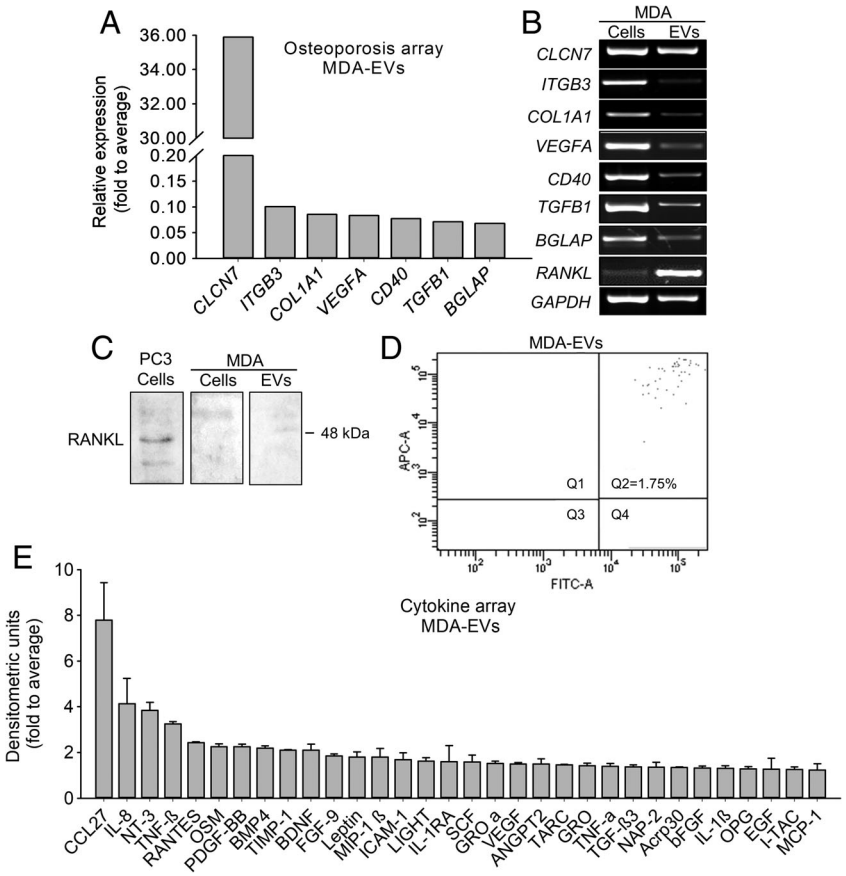

Fig. 1. Transcriptional and cytokine profile of MDA-EVs. (*A*) Human osteoporosis real-time array performed on 0.1 μg of reverse-transcribed RNA extracted from MDA-EVs and subjected to a preamplification step. (*B*) Semiquantitative RT-PCR performed on 1 μg of reverse-transcribed RNA extracted from MDA-MB-231 (MDA) cells or derived EVs. (*C*) Western blot analysis to evaluate RANKL expression in PC3 cells (50 μg proteins) as positive control, MDA cells (50 μg proteins). and MDA-EVs (5 μg proteins). (*D*) Cytofluorometric analysis of RANKL-positive EVs isolated from MDA-MB-231 cells (12 mL of CM collected from one 175-cm^2 flask, cell density $6.5 \times 10^4/cm^2$). (*E*) Cytokine array performed on MDA-EVs protein lysates (15 μg). Result in *A* is from one MDA-EVs preparation; results in *B–E* are representative or *E* the mean ± SD of at least three independent preparations of MDA cells and/or MDA-derived EVs.

preosteoclast fusion, respectively. Among the genes related to osteoblast functions, we found *COL1A1* and *BGLAP* (Fig. 1*A*,*B*). Transcriptional expression of *Transforming Growth Factor beta 1* (*TGFB1*) and *VEGF* were also found (Fig. 1*A*,*B*). This profile generally mirrors the transcriptional content of the cells (Supplementary Fig. 5*E* and Fig. 1*B*); there are, however, some exceptions. An intriguing example is *RANKL*: although its expression is barely detectable in MDA cells, high levels of this mRNA were observed in MDA-EVs (Fig. 1*B*). However, Western blot on MDA-EVs did not show any positive signal for RANKL (Fig. 1*C*), whereas cytofluorometric analysis revealed a negligible percentage of RANKL-positive MDA-EVs (Fig. 1*D*).

Finally, to characterize the cytokine profile of MDA-EVs, they were subjected to molecular profiling by a human cytokine antibody array (Fig. 1*E*). CCL27 (alias CTACK), which is a positive regulator of breast cancer aggressiveness,[22] was the most expressed cytokine. Among the well-expressed cytokines, there were some factors known to foster osteoclastogenesis, including IL8, Macrophage Inflammatory Protein (MIP)-1α (alias CCL3) and MIP-1β (alias CCL4), and Platelet-Derived Growth Factor (PDGF)-BB,[23–26] whereas, among the angiogenic cytokines, we observed Angiopoietin 2 and VEGF. Of note, MIP-1α and PDGF-BB are also negative regulators of osteoblast differentiation.[27,28]

Another cytokine expressed by MDA-EVs was oncostatin M (OSM), which potentiates preintravasation of breast cancer cells and their ability to metastasize the lung and the bone.[29,30]

Effect of breast cancer–derived EVs on osteoblast behavior

We next investigated whether EVs could be responsible for the changes induced by MDA CM in osteoblasts. Interestingly, MDA-EVs reduced osteoblast metabolic activity and number (Fig. 2*A*,*B*) as well as Alp activity (Fig. 2*C*) compared to untreated osteoblasts. *Cyclin D1* mRNA expression was also significantly reduced, along with *Alp*, *Runx2*, *Osx*, *Bglap*, and *Col1a1* (Fig. 2*D*). Similar results were observed when osteoblasts were treated with MCF7-derived EVs (Fig. 2*E–H*).

When we looked at the cytokines regulating osteoclastogenesis, an increase of *Rankl* and a decrease of *Opg* and *M-csf* mRNAs were observed in MDA-EV–treated osteoblasts (Fig. 3*A*). Moreover, MDA-EVs enhanced *Il1b*, *IL6*, *Lcn2*, and *Nos2* expression (Fig. 3*B*). Similar results were found in MCF7-EVs–treated osteoblasts (Fig. 3*C*,*D*).

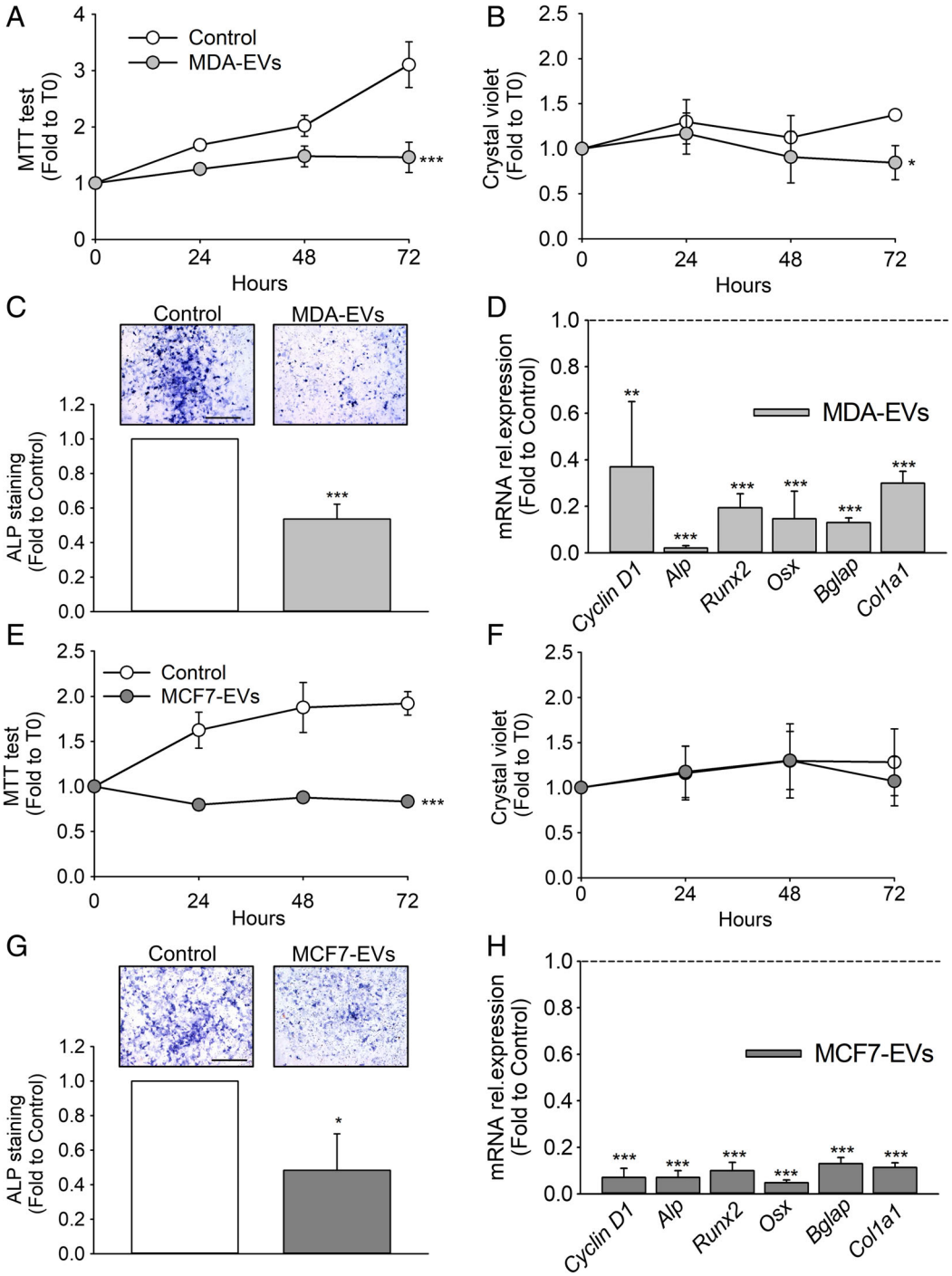

Fig. 2. Effect of breast cancer–derived EVs on osteoblast differentiation. (*A–D*) Mouse primary osteoblasts were starved overnight in serum-free DMEM and treated with DMEM as control or with EVs isolated from the CM of the human breast cancer cell line MDA-MB-231 (MDA-EVs, 12 mL collected from one 175-cm^2 flask, cell density 6.5 × 10^4 cells/cm^2). (*A*) Cell metabolic activity evaluated by the MTT assay and (*B*) quantification of cell number by crystal violet staining at the times indicated in the abscissa. (*C*) Alkaline phosphatase (Alp) activity evaluated after 48 hours by cytochemical assay. (*D*) RNA was extracted and subjected to real-time RT-PCR to evaluate the expression of *Cyclin D1*, and of the osteoblast differentiating genes *Alp*, Runt-related transcription factor 2 (*Runx2*), Osterix (*Osx*), Osteocalcin (*Bglap*), and Collagen 1a1 (*Col1a1*). (*E–H*) Mouse primary osteoblasts were starved overnight in serum-free DMEM and treated with DMEM as control or with EVs isolated from the CM of the human breast cancer cell line MCF7 (MCF7-EVs, 12 mL collected from one 175-cm^2 flask, cell density 4.5 × 10^4 cells/cm^2). (*E*) Cell metabolic activity evaluated by the MTT assay and (*F*) quantification of cell number by crystal violet staining at the times indicated in the abscissa. (*G*) Alkaline phosphatase (Alp) activity evaluated after 48 hours by cytochemical assay. (*H*) RNA was extracted and subjected to real-time RT-PCR to evaluate the expression of *Cyclin D1*, and of the osteoblast differentiating genes *Alp*, *Runx2*, *Osx*, *Bglap*, and *Col1a1*. Results are the mean ± SD of three independent experiments (*A,B,E*: $*p = 0.01$ and $***p < 0.001$ versus control, AUC; *C,D,G,H*: $*p < 0.05$, $**p = 0.008$, and $***p < 0.001$ versus control, Student's *t* test, dot line = control set at 1; bar = 500 μm).

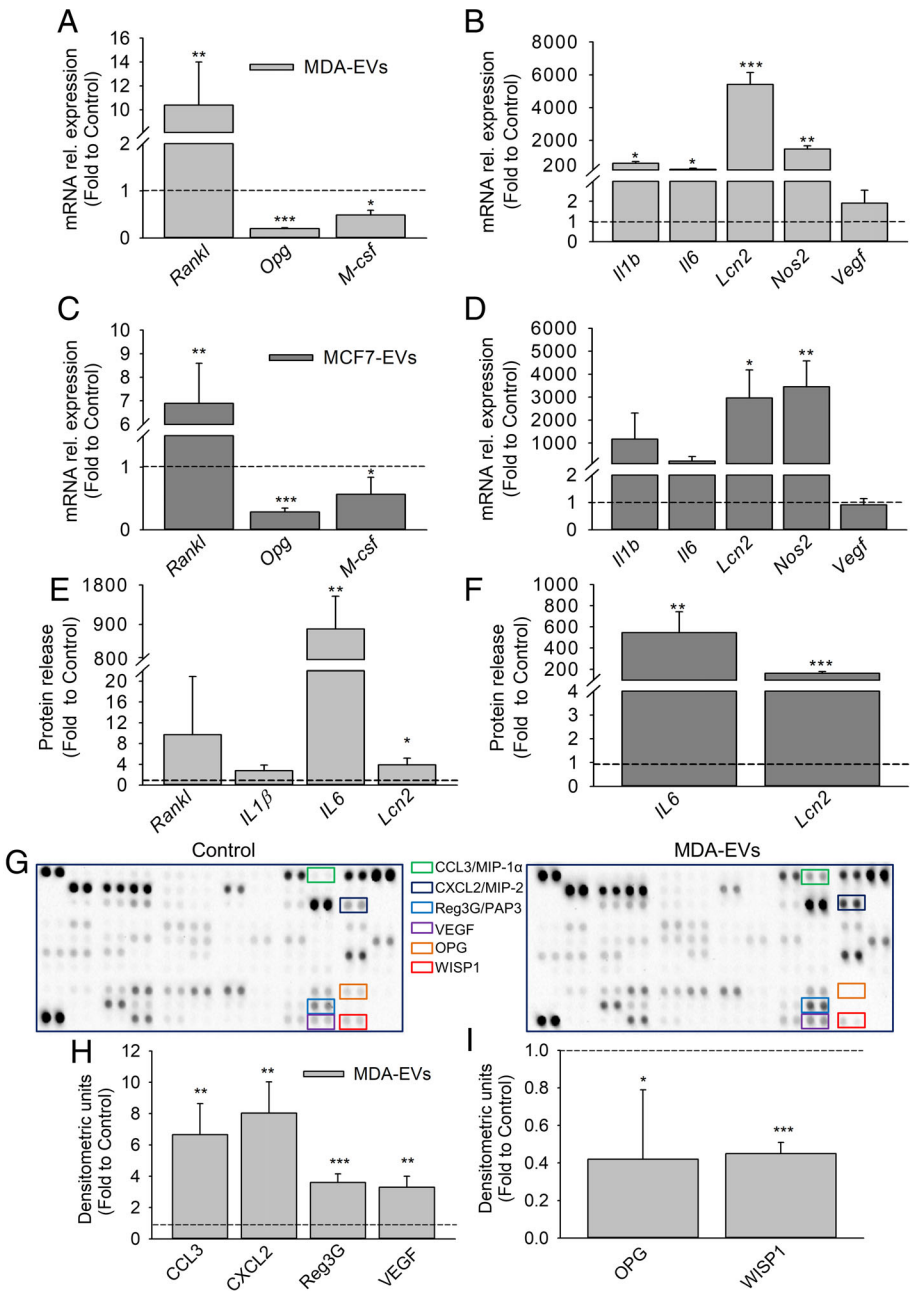

Fig. 3. Effect of breast cancer–derived EVs on osteoblast cytokine profile. (*A–D*) Mouse primary osteoblasts were starved overnight in serum-free DMEM and treated with DMEM as control or with EVs isolated from the CM of (*A,B*) MDA-MB-231 (MDA-EVs, 12 mL collected from one 175-cm^2 flask, cell density 6.5 × 10^4 cells/cm^2) or (*C,D*) MCF7 (MCF7-EVs, 12 mL collected from one 175-cm^2 flask, cell density 4.5 × 10^4 cells/cm^2). (*A,C*) Transcriptional expression of the cytokines regulating osteoclastogenesis indicated in the abscissa and of (*B,D*) *Il1b*, *Il6*, *Lcn2*, *Nos2*, and *Vegf* evaluated by real-time RT-PCR. (*E,F*) ELISA assay to determine the release of the cytokines indicated in the abscissa in the CM of osteoblasts left untreated or treated with (*E*) MDA-EVs or (*F*) MCF7-EVs. (*G–I*) Mouse primary osteoblasts were starved overnight in serum-free DMEM and treated with DMEM as control or with MDA-EVs. After 48 hours the CM was collected from osteoblasts and subjected to cytokine array. (*G*) Representative pictures showing the membranes incubated with CM from control osteoblasts (left) or osteoblasts treated with MDA-EVs (right). (*H,I*) Densitometric analysis showing the cytokines modulated by MDA-EVs treatment, as a result of the densitometric analysis of the spots of interest normalized for the housekeeping proteins. Results are (*G*) representative or (*A–F,H,I*) the mean ± SD of three independent experiments (*$p < 0.05$, **$p < 0.01$, and ***$p < 0.001$ versus control, Student's *t* test; dot line = control set at 1).

To assess whether these differences were mirrored also at protein level, we performed ELISA assays on CM collected from EV-treated osteoblasts, finding a trend of increase of RANKL and IL1β release, whereas a significant increase of IL6 and Lcn2 were observed in osteoblasts treated with MDA-EVs (Fig. 3*E*). Similar results were observed with MCF7-EVs (Fig. 3*F*) and with 4T1-EVs (Supplementary Fig. 6).

To broadly investigate the impact of breast cancer cell–derived EVs on the release of cytokines by osteoblasts, we subjected the CM collected from untreated or MDA-EV–treated

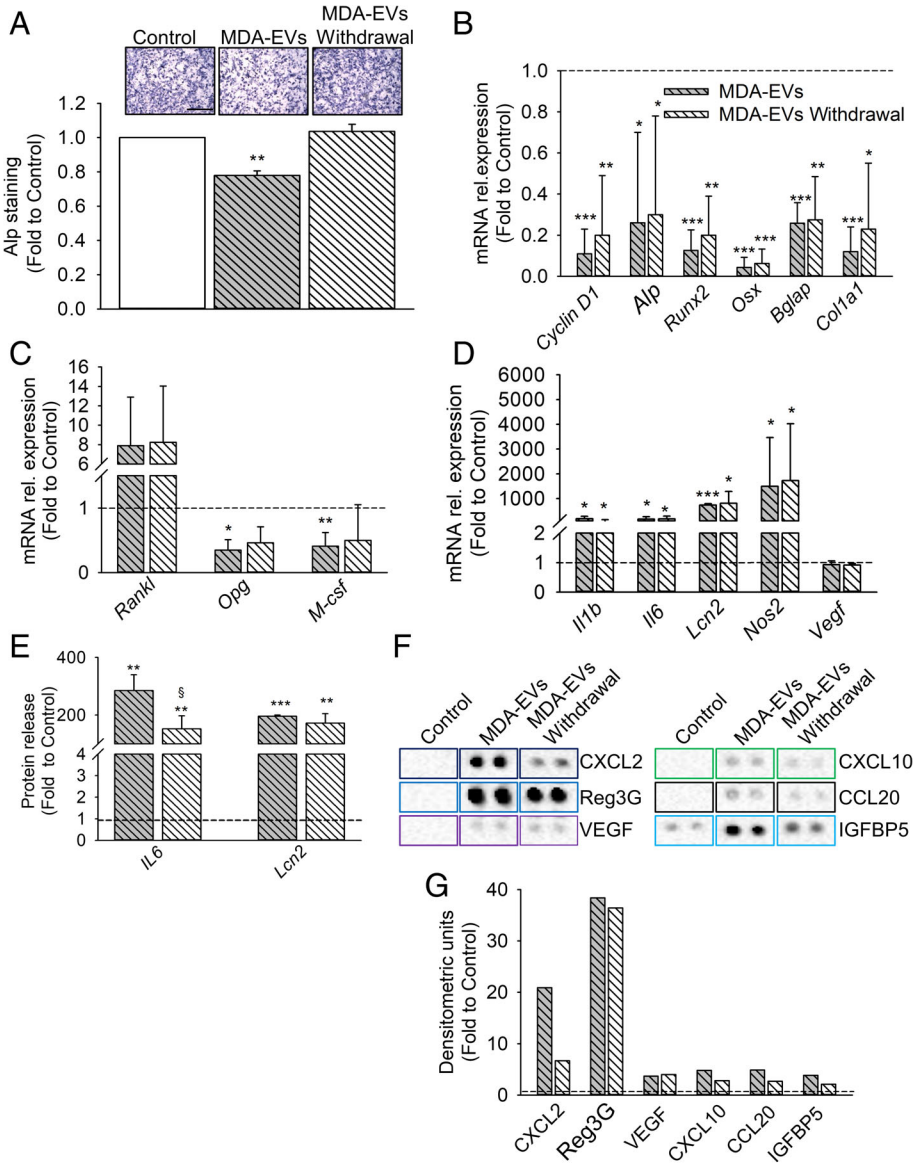

Fig. 4. Persistence of MDA-EVs mediated effects on osteoblasts. Mouse primary osteoblasts were starved overnight in serum-free DMEM and treated for 96 hours with DMEM (control), MDA-EVs (12 mL of CM collected from one 175-cm^2 flask, cell density 6.5 × 10^4 cells/cm^2), or with MDA-EVs for 48 hours followed by DMEM for additional 48 hours after washing (MDA-EVs withdrawal). (*A*) Alp activity evaluated by cytochemical assay. (*B–D*) RNA was extracted and subjected to real-time RT-PCR to evaluate the expression of (*B*) *Cyclin D1* and of the osteoblast-differentiating genes *Alp*, *Runx2*, *Osx*, *Bglap*, and *Col1a1*. (*C*) Transcriptional expression of the cytokines regulating osteoclastogenesis indicated in the abscissa and of (*D*) *Il1b*, *Il6*, *Lcn2*, *Nos2*, and *Vegf* evaluated by real-time RT-PCR. (*E*) ELISA assay to determine the release of the IL6 and Lcn2 by osteoblasts. Results are the mean ± SD of three independent experiments (*$p < 0.05$, **$p < 0.01$, and ***$p < 0.001$ versus control, $^{§}p = 0.032$ versus MDA-EVs, Student's *t* test; bar = 500 μm). (*F,G*) Mouse cytokine array performed on the CM of osteoblasts treated as in *A*. (*F*) Representative dot plots for the indicated cytokines. (*G*) Densitometric analysis of the dots in *F* normalized for the housekeeping proteins. In *F* and *G*, results are from one cytokine array incubated with a pool of CM collected from three independent experiments.

osteoblasts to a cytokine array, which allows simultaneous detection of important cytokines, chemokines, and growth factors influencing tumor growth. Along with the observed increase of IL6 and Lcn2 release (Fig. 3*E*), MDA-EV treatment stimulated osteoblast release of C-C motif Chemokine Ligand (CCL)-3 (alias MIP-1α), CXC motif, Chemokine Ligand (CXCL)-2 (alias MIP-2), Regenerating islet-derived protein 3 Gamma (Reg3G), and VEGF (Fig. 3*G,H*), and decreased OPG and WISP1 (WNT1 Inducible Signaling Pathway Protein 1) release (Fig. 3*G,I*). CCL3 has been implicated in the progression of triple-negative breast cancers[31] and in the induction of osteoclastogenesis.[23] Similarly, CXCL2 favors tumor angiogenesis and tumor-associated osteolysis.[32–35] OPG

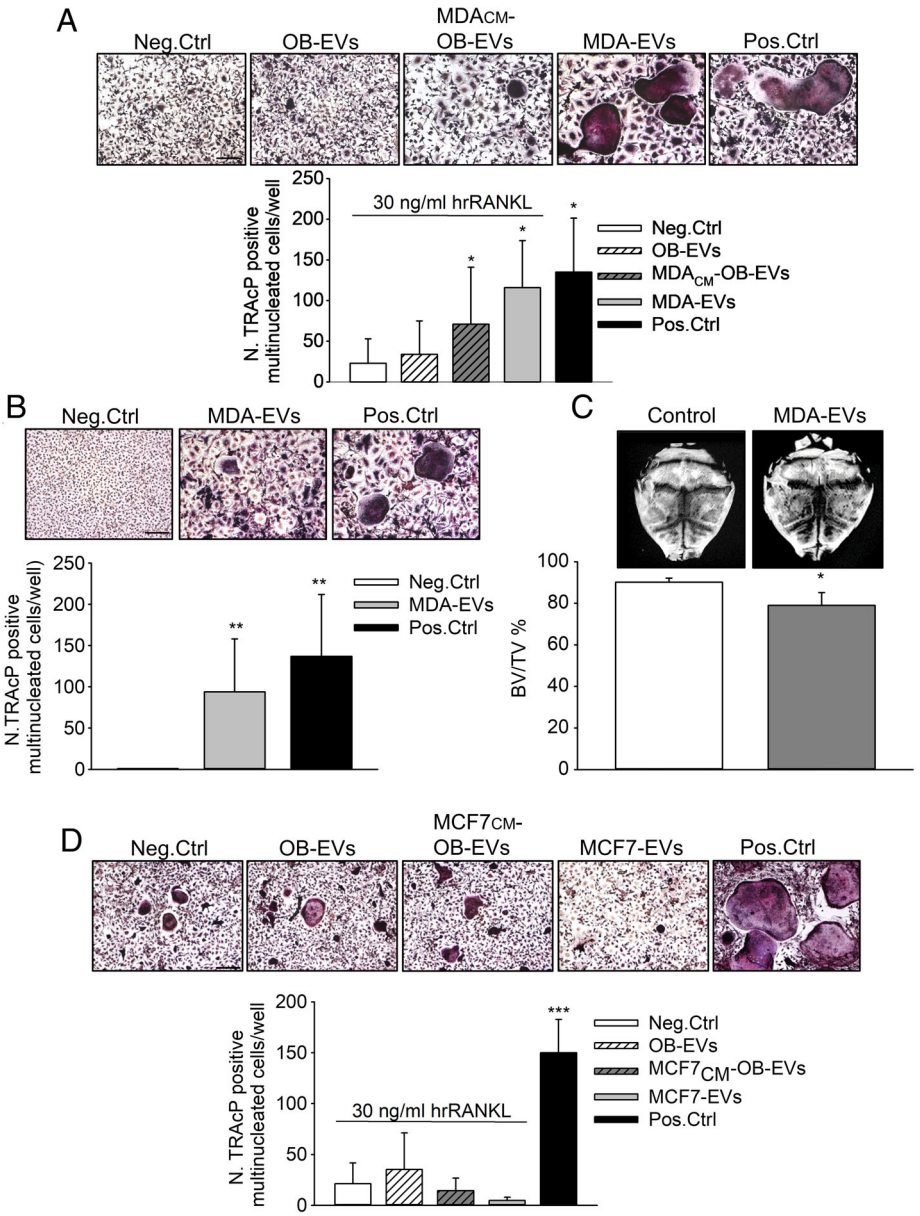

Fig. 5. Effect of osteoblast-EVs and breast cancer cell–EVs on osteoclastogenesis. (*A*) Mouse bone marrow mononuclear cells were untreated (Neg.Ctrl), treated with osteoblast EVs (OB-EVs, 6 mL of CM from one 75-cm^2 Petri dish, 3.5 × 10^4 cells/cm^2) or with EVs isolated from osteoblasts pretreated with MDA-CM (MDA_{CM}-OB-EVs) and with MDA-EVs (6 mL of CM from one 75-cm^2 Petri dish, cell density 6.5 × 10^4 cells/cm^2) in the presence of suboptimal concentrations of hrRANKL (30 ng/mL). (*B*) Osteoclast primary cultures from mouse bone marrow were untreated (Neg.Ctrl) or treated with MDA-EVs without suboptimal concentrations of hrRANKL. (*C*) μCT analysis performed on ex vivo mouse calvariae cultures treated with MDA-EVs (12 mL of CM from one 175-cm^2 flask, cell density 6.5 × 10^4 cells/cm^2). (*D*) Mouse bone marrow mononuclear cells were untreated (Neg. Ctrl), treated with OB-EVs (6 mL of CM from one 75-cm^2 Petri dish, cell density 3.5 × 10^4 cells/cm^2), with EVs isolated from osteoblasts pretreated with MCF7-CM ($MCF7_{CM}$-OB-EVs) or with MCF7-EVs (6 mL of CM from one 75-cm^2 Petri dish, cell density 4.5 × 10^4 cells/cm^2) in the presence of suboptimal concentrations of hrRANKL (30 ng/mL). Positive control (Pos.Ctrl) =120 ng/mL hrRANKL. Data is the mean ± SD of (*A*,*B*,*D*) three independent experiments or (*C*) 3 mice/group (*$p < 0.05$, **$p < 0.01$, and ***$p < 0.001$ versus Neg.Ctrl; Student's *t* test, bar = 50 μm).

is the decoy receptor that binds Rankl and blocks its interaction with Rank; therefore, its reduced secretion favors osteoclastogenesis. Finally, WISP1 has been identified as a tumor suppressor factor in breast cancer,[36] whereas Reg3G, an extracellular protein known for its antibacterial properties,[37] has recently been reported to be implicated in pancreatic carcinogenesis.[38]

We next asked whether the factors modulated by MDA-EVs in the osteoblast secretome were also present in the EV fraction, but this was ruled out because neither naïve OB-EVs nor OB-EVs derived from osteoblasts treated with MDA-EVs expressed these cytokines (Supplementary Fig. 7). However, naïve OB-EVs contained Angiopoietin like 3 (ANGPTL3) and IL33, whereas

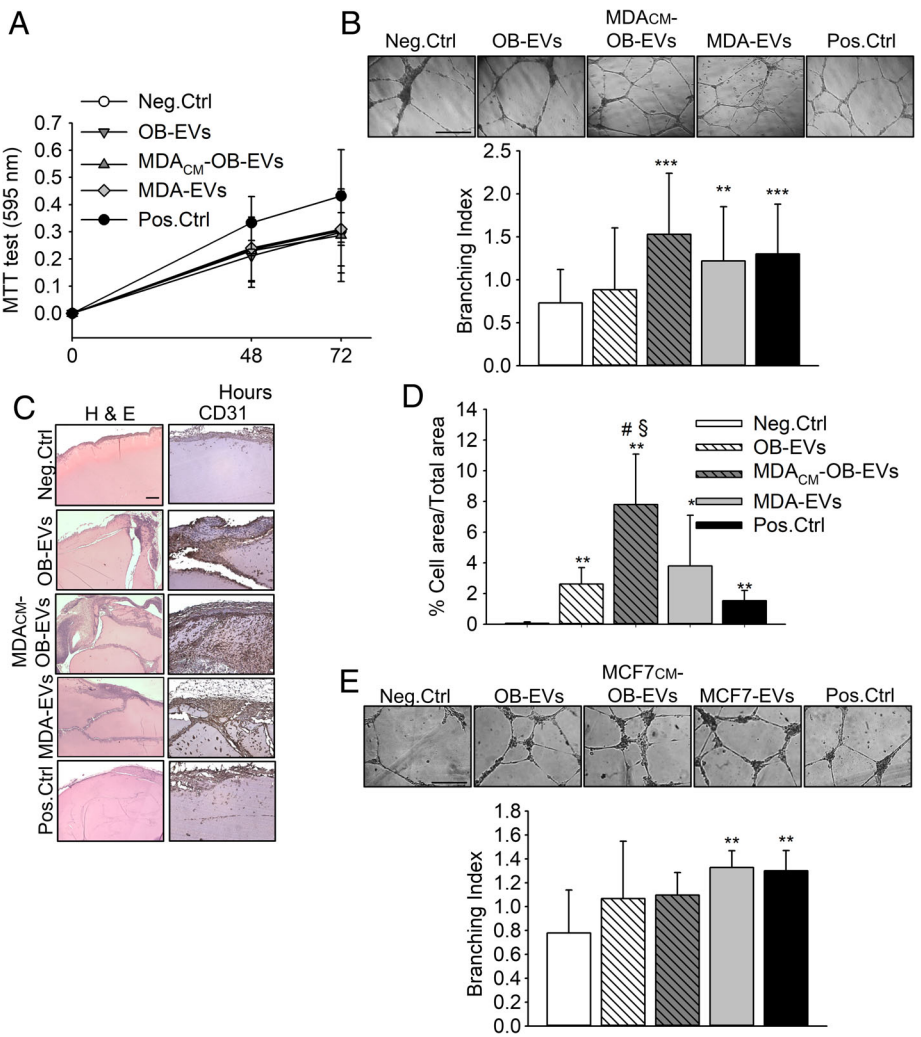

Fig. 6. Effect of osteoblast-EVs and breast cancer cell–EVs on angiogenesis. (*A*,*B*) Human umbilical vein endothelial cells (HUVECs) were treated with OB-EVs (6 mL of CM from one 75-cm^2 Petri dish, cell density 3.5 × 10^4 cells/cm^2), or with EVs isolated from osteoblasts pretreated with MDA-CM (MDA$_{CM}$-OB-EVs) and with MDA-EVs (6 mL of CM from one 75-cm^2 Petri dish, cell density 6.5 × 10^4 cells/cm^2). (*A*) HUVECs Cell metabolic activity was evaluated by the MTT assay after treatment with vehicle (Neg.Ctrl), osteoblast EVs (OB-EVs), EVs isolated from osteoblasts pretreated with MDA-CM (MDA$_{CM}$-OB-EVs), MDA-EVs or endothelial growth medium (EGM)-2 (Pos.Ctrl). (*B*) in vitro tube formation assay (branching index) performed on HUVEC cells treated as described in *A*. (*C*,*D*) in vivo Matrigel plug assay performed by subcutaneous injection of 8-week-old male mice with 0.5 mL of Matrigel, enriched with PBS (Neg.Ctrl), OB-EVs, MDA$_{CM}$-OB-EVs, or 50 ng/mL of ECGS + 150 ng/mL VEGF (Pos.Ctrl). (*C*) Hematoxylin and eosin staining and immunohistochemistry for the endothelial marker CD31. (*D*) Quantification of the percent of cell area over the total area of the plug. (*E*) in vitro tube formation assay (branching index) performed on HUVECs untreated or treated with osteoblast EVs (OB-EVs, 6 mL of CM from one 75-cm^2 Petri dish, cell density 2.5 × 10^4 cells/cm^2), EVs isolated from osteoblasts pretreated with MCF7-CM (MCF7$_{CM}$-OB-EVs), MCF7-EVs (6 mL of CM from one 75-cm^2 Petri dish, cell density 4.5 × 10^4 cells/cm^2), or with endothelial growth medium (EGM)-2 (Pos.Ctrl). Data are the mean ± SD of (*A*,*B*,*E*) three independent experiments or (*C*,*D*) of 5 mice/group (**$p < 0.01$ and ***$p < 0.001$ versus Neg.Ctrl; $^{\#}p = 0.004$ versus OB-EVs, $^{\S}p = 0.001$ versus Pos.Ctrl, Student's *t* test, in *C*,*D*) bar = 200 μm). ECGS = endothelial cell growth supplement.

expression of CXCL5 was observed only in EVs isolated from osteoblasts educated by MDA-EVs (Supplementary Fig. 7).

Finally, we investigated whether the effect of MDA-EVs was persistent or it could be rescued after EV withdrawal. To this aim, osteoblasts were treated with MDA-EVs for 48 hours, then they were subjected to extensive washes to remove the EVs and cultured for additional 48 hours in DMEM. Although we observed a recovery of Alp activity after MDA-EV removal (Fig. 4*A*), the effects of MDA-EVs on transcriptional expression of osteoblast-differentiating and cytokines genes were persistent (Fig. 4*B-D*). When we looked at protein level, we found a partial recovery of the increased IL6 release (Fig. 4*E*) and of CXCL2 (Fig. 4*F* left panel and Fig. 4*G*), thus indicating that the MDA-EV effect is mostly persistent over the timeframe of our experiment. Treatment of MDA-EVs for 96 hours instead of 48 hours also increases the release of CXCL10, CCL20, and IGFBP5 (Fig. 4*F* right panel; Fig. 4*G*); however, a partial rescue after withdrawal of EVs was only observed for the latter (Fig. 4*F* right panel; Fig. 4*G*).

Taken together, these results demonstrate the ability of MDA-EVs to influence osteoblast behavior by promoting the secretion

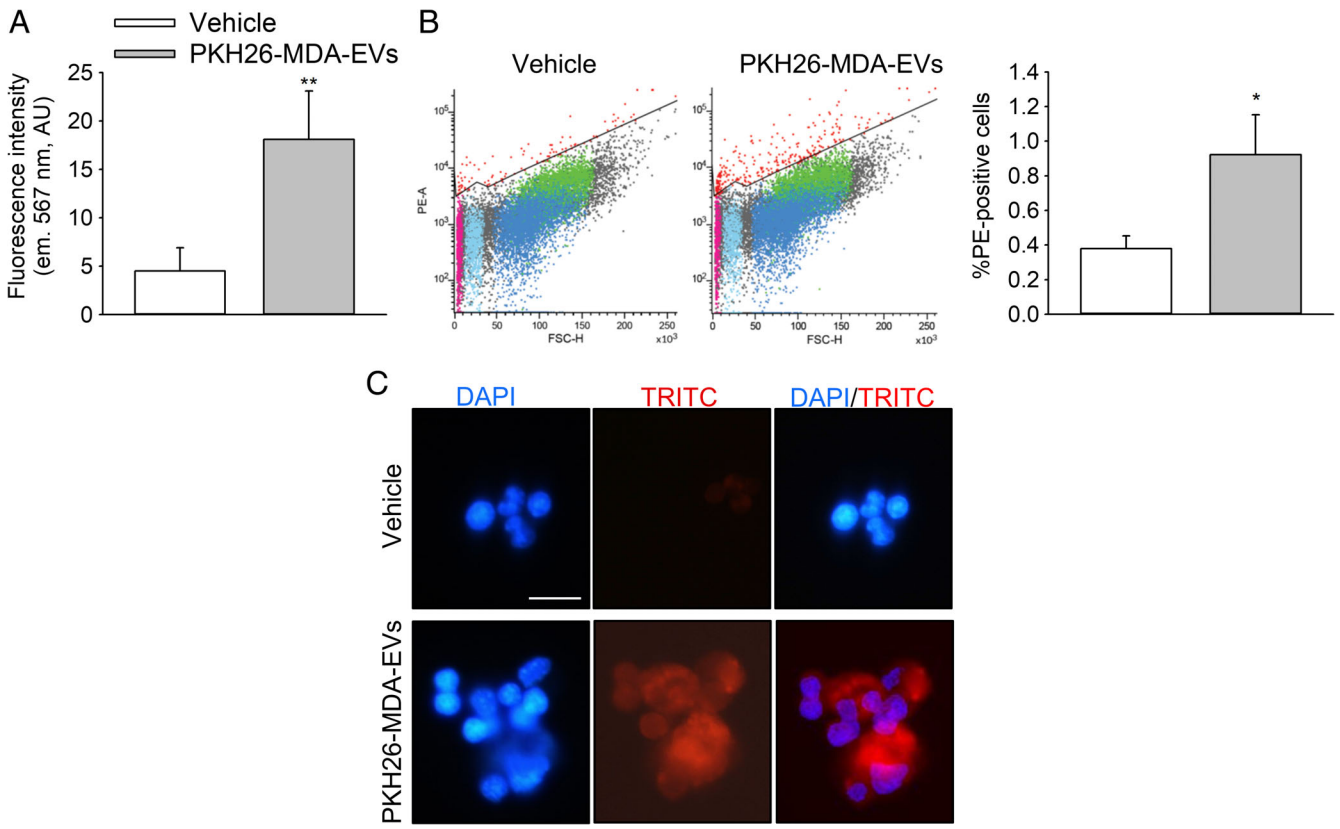

Fig. 7. In vivo tumor cell–EVs targeting the bone. Seven-day-old mice were intraperitoneally injected with MDA-EVs (12 mL of CM collected from one 175-cm^2 flask, cell density 6.5 × 10^4 cells/cm^2 injected to each mouse) labeled with the PKH26 fluorophore (PKH26-MDA-EVs) or with PBS (vehicle). After 5 hours, mice were euthanized and bones (forelimbs, hindlimbs, and calvariae) explanted and subjected to lipid extraction for fluorimetric analysis, cryosectioning, and confocal microscopy, while BM was flushed out for FACS analysis. (*A*) Fluorimetric quantification of PKH26 in lipid extracts. (*B*) Representative dot plot and quantification (graph) of % of fluorescent cells, as determined with PE filter, in whole BM flushed out cells. (*C*) PE-high BM cells from PKH-MDA-EVs-injected mice were sorted onto polylysine slides by FACS, along with random BM cells from vehicle-injected mice. After mounting with DAPI, cells were observed by conventional epifluorescence. Data are the mean ± SD of (*A*) 4 mice/group and (*B*,*C*) 5 mice/group (*$p < 0.02$ and**$p = 0.008$ versus vehicle, Student's *t* test; bar = 25 μm). BM = bone marrow.

of pro-tumoral factors and reducing the secretion of anti-osteoclastogenic factors.

Breast cancer cell–EVs and OB-EVs educated by tumor cell CM stimulate osteoclastogenesis

Osteoblasts induce osteoclastogenesis through the production of several cytokines, including Rankl, and an exacerbated osteoclast activity is the primary cause of bone metastasis–induced osteolysis. To assess whether EVs were involved in this phenomenon, we tested the effect of EVs isolated from osteoblast CM (OB-EVs) on osteoclastogenesis. Mouse primary osteoclasts were differentiated from the fraction of the bone marrow enriched in the monocyte/macrophage subpopulation in the presence of OB-EVs. Although this treatment did not induce osteoclastogenesis, a significant increase of TRAcP-positive mononuclear cells was observed upon treatment with OB-EVs isolated from osteoblasts preincubated with MDA-MB-231 CM (MDA_{CM}-OB-EVs, Supplementary Fig. 8). We therefore decided to repeat the experiment in the presence of suboptimal concentrations of hrRANKL (30 ng/mL). In these conditions, OB-EVs had no effect on osteoclastogenesis, whereas MDA_{CM}-OB-EVs significantly stimulated osteoclast formation (Fig. 5*A*).

Interestingly, we observed that MDA-EVs also induced osteoclastogenesis in the absence of RANKL (Fig. 5*B*), thus indicating that the exogenous RANKL cytokine is dispensable for the osteoclastogenic effect of MDA-EVs. To complete this picture, we performed an ex vivo experiment of calvaria culture in the presence of MDA-EVs, finding that this treatment reduced the bone volume/tissue volume (BV/TV %) (Fig. 5*C*). In contrast, when we employed MCF7-CM to educate OB-EVs or MCF7-EVs, we did not find any effect on osteoclastogenesis (Fig. 5*D*).

Finally, we assessed whether co-treatment with OB-EVs and MDA-EVs could have a synergic effect on osteoclastogenesis compared to single treatments. In this circumstance, we confirmed the effects observed with the single MDA-EVs treatment and found no further enhancement of osteoclastogenesis with the co-treatment (Supplementary Fig. 9*A*).

Taken together, these results indicate that factors released by MDA-MB-231 cells increase the ability of OB-EVs to stimulate osteoclastogenesis.

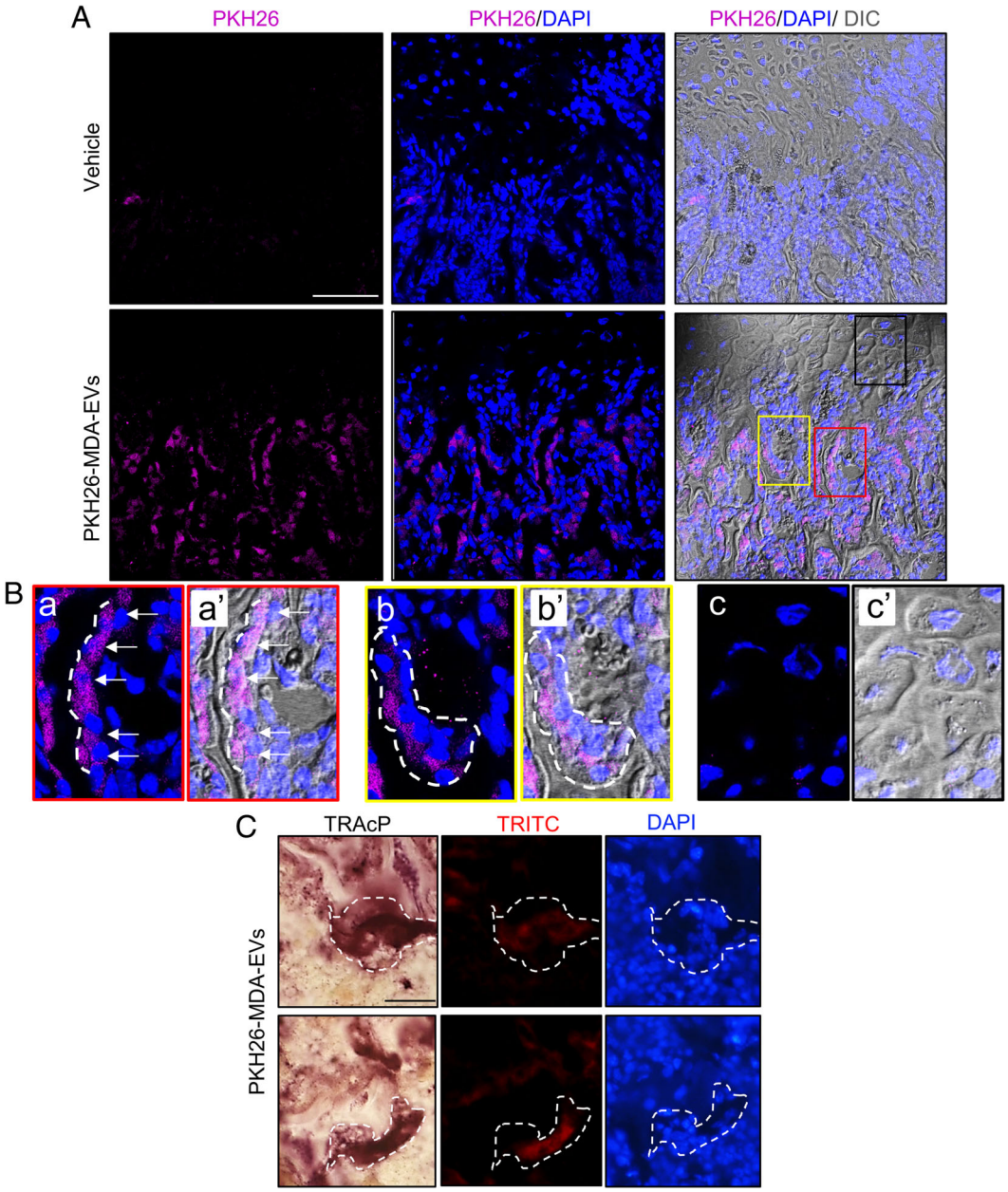

Fig. 8. In vivo tumor cell–EVs targeting the bone. Seven-day-old mice were intraperitoneally injected with MDA-EVs (12 mL of CM collected from one 175-cm^2 flask, cell density 6.5 × 10^4 cells/cm^2 injected to each mouse) labeled with the PKH26 fluorophore (PKH26-MDA-EVs) or with PBS (vehicle). After 5 hours, mice were euthanized and femurs and calvariae were collected and fixed in 4% buffered PFA. (*A*) Femur cryosections were mounted with DAPI and observed by confocal microscopy. (*B*) Magnification of *A* showing representative images of (a, a′) osteoblasts, (b, b′) osteoclasts and (c, c′) chondrocytes shown as (a, b, c) PKH26/DAPI or (a′, b′, c′) PKH26/DAPI/DIC merge images. (*C*) Representative pictures of femur cryosections observed by epifluorescence microscopy to detect DAPI and PKH26 signal and stained for TRAcP activity. Images are representative of 5 mice/group (*A*: bar = 80 μm; *B*: bar = 20 μm; *C*: bar = 25 μm).

Breast cancer cell–EVs and OB-EVs educated by tumor cells CM stimulate angiogenesis

Another cell population present in the bone microenvironment and participating in local tumor growth are endothelial cells. We therefore investigated the effect of OB-EVs and breast cancer cell–EVs on HUVEC behavior. OB-EV treatment did not affect cell metabolic activity, evaluated by the MTT assay (Fig. 6*A*), nor in vitro tube formation (Fig. 6*B*), whereas a significant increase in percent of tube branching was observed when treating with MDA_{CM}-OB-EVs or with MDA-EVs (Fig. 6*B*). Interestingly, when we performed in vivo Matrigel plug assays, OB-EVs significantly increased angiogenesis, evaluated by determination of the percent of the area covered by migrated endothelial cells over the total area of the plugs (Fig. 6*C*,*D*). This angiogenic effect of OB-EVs was much more powerful after pretreatment of osteoblasts with MDA-CM (Fig. 6*D*, *E*). Consistent with the in vitro results, a direct effect of MDA-EVs on in vivo angiogenesis was also observed (Fig. 6*D*,*E*).

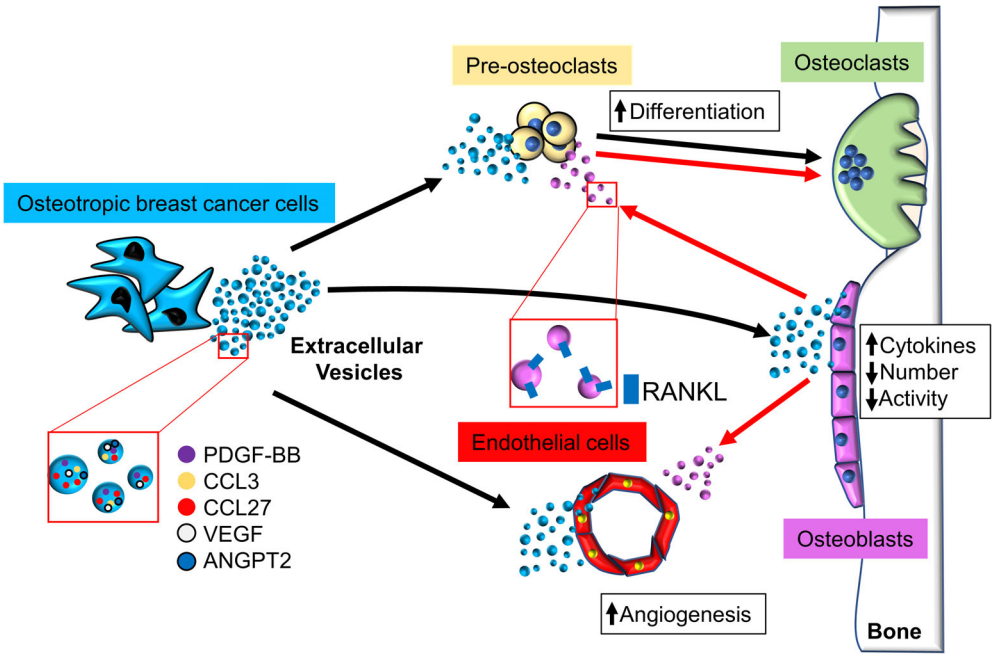

Fig. 9. Proposed EV-mediated communication mechanism among cancer cells and bone cells. Osteotropic breast cancer cells release EVs that contain several molecular mediators, including PDGF-BB, CCL3, CCL27, VEGF, and ANGPT2. Cancer EVs exert several actions in the bone microenvironment: they target preosteoclasts and stimulate their differentiation to multinucleated OCs, osteoblasts increasing their cytokine production, while reducing their number and activity, and endothelial cells, which increases angiogenesis. Furthermore, cancer-released factors can increase osteoblast production of RANKL-positive EVs, which further stimulate osteoclastogenesis and angiogenesis. This series of changes mediated by breast cancer cells EVs result in a deep reprogramming of the bone microenvironment, which makes it more favorable for cancer growth and engraftment.

Similarly, an increase of in vitro tube formation was observed with EVs isolated from MCF7-CM which, however, failed to educate OB-EVs toward a proangiogenic effect (Fig. 6*E*). Moreover, the combination treatment with OB-EVs plus MDA-EVs did not further increase in vitro angiogenesis (Supplementary Fig. 9*B*).

In vivo breast cancer cell–EV integration into the bone tissue

Having shown a clear effect of breast cancer–derived EVs on in vitro bone cells, we finally evaluated whether they were able to target and integrate into the bone tissue in vivo. As already shown for OB-EVs,[13] we performed intraperitoneal injection of 7-day-old mice with MDA-EVs preincubated with the lipophilic fluorophore PKH26 observing, after 5 hours, a significantly higher fluorescent signal in their bones compared to bones collected from mice inoculated with PBS as vehicle (Fig. 7*A*). We flushed out the BM and analyzed BM cells by cytofluorometry, using the PE filter set, and found a significantly higher signal in BM cells recovered from PKH26-MDA-EV–injected mice compared to controls (Fig. 7*B*). However, the percentage of positive cells/total cells was low (~1%), suggesting that a small subgroup of BM cells was targeted by the MDA-EVs. Slides of sorted BM cells also confirmed the presence of PKH26-positive cells (Fig. 7*C*).

Finally, we analyzed cryosections of femurs explanted from PKH26-MDA-EVs or vehicle-injected mice by confocal microscopy (Fig. 8*A*). We observed that cells lining the trabecular bone were highly PKH26-positive in MDA-EV–injected mice (Fig. 8*A*). They included cells morphologically reminiscent of osteoblasts (Fig. 8*B*, a-a′) and multinucleated osteoclasts (Fig. 8*B*, b-b′). In contrast, chondrocytes were negative (Fig. 8*B*, c-c′). TRAcP histochemical assay on the same sections confirmed the co-localization of the PKH26 signal with TRAcP-positive multinucleated cells (Fig. 8*C*).

Taken together, these results showed that MDA-EVs target the bone microenvironment and are primarily taken up by osteoclasts, osteoblasts, and a few BM cells.

Discussion

Bone metastases represent a frequent complication in advanced breast cancer, with an occurrence of up to 70%.[1] Tumor cells generate a favorable premetastatic niche prior to their dissemination, and this process is at least in part mediated by EVs.[39,40] Because we have previously shown that bone cells crosstalk via EVs,[13] we hypothesized that EV-mediated communication between breast cancer cells and bone cells could play a role in cancer progression. In agreement with this hypothesis, we found that breast cancer cell–EVs influence bone-resident cells both directly and indirectly. In particular, these EVs inhibited osteoblast differentiation and reduced cell number and activity, while increasing osteoclast formation in a RANKL-independent manner. Angiogenesis was also found to be increased by MDA-EVs both in vitro and in vivo. However, alteration of the crosstalk among bone-resident cells was also observed, because in

osteoblasts breast cancer cell–EVs enhanced the transcription and the secretion of pro-angiogenic, pro-inflammatory, and pro-osteoclastogenic factors, which eventually increased angiogenesis and osteoclastogenesis, at least in part through tumor-educated OB-EVs.

Direct effects on osteoblasts by MDA-EVs are likely to depend on their ability to inhibit the expression of osteoblast-specific genes, including the two master transcription factors, Runx2 and Osx, as well as the mature osteoblast markers *Alp*, *Bglap*, and *Col1a1*. Furthermore, the reduction in osteoblast number could be due to an induction of cell cycle arrest, as indicated by the decrease of *Cyclin D1* mRNA expression by MDA-EVs. The underlying pathways remain to be elucidated. However, we could hypothesize the involvement of the NF-κB, which would be a strong candidate given that many of its downstream targets (Il6, Il1B, Lcn2, Nos2, RANKL, CCL3, and Vegf) were strongly increased at the transcriptional and/or protein level. Although more experiments are needed to confirm the implicated molecular mechanisms, the effects appear to converge on a strong reduction of osteoblast growth, activity, and differentiation.[41–44]

We also asked whether removing MDA-EVs from osteoblasts after 48 hours of treatment would result in a rescue of the observed changes in the osteoblast phenotype, finding that most of the effects exerted by MDA-EVs persist, regardless of EV removal, even at 96 hours. This might be explained by the fact that internalized EV cargo has a turnover inside the target cell, which may be longer than 48 hours. Notable exceptions include IL6, CXCL2, and IGFBP5, all showing a partial rescue, whereas a total rescue was observed for Alp activity.

Osteoclastogenesis induced by cancer cell EVs seems to be linked to RANKL in different ways. Our data shows that although MDA-EVs are RANKL-negative, they are highly enriched in mRNA coding for this factor, even compared to MDA cells. We can speculate that this mRNA can be an educating factor, potentially taken up and translated by the bone resident cells, thus contributing to the increase of osteoclastogenesis. This result is consistent with reports demonstrating functionality of proteins arising from exosomal mRNA translation.[9,45] In addition, it is interesting to note that MDA-EVs can induce osteoclastogenesis despite being RANKL-negative. Furthermore, treating osteoclast precursors with MDA-EVs without exogenous RANKL still results in mature osteoclast formation. These results suggest that MDA-EVs foster RANKL-independent osteoclastogenesis. We can hypothesize that this process might be promoted by the shuttling of inflammatory factors that are also known to be strong inducers of osteoclastogenesis, such as IL6, IL1B, IL8, CCL3, CCL4, and PDGF-BB.

In this study, we also showed that cancer cell EVs were able to activate angiogenesis by a direct mechanism. This functional data is supported by the molecular profile of MDA-EVs, which contains pro-angiogenic mRNAs (*TGFB1*, *VEGF*) and proteins (Angiopoietin 2, VEGF). However, indirect effects are also present, showing how cancer cell EVs can deeply reprogram the bone microenvironment and alter the physiological crosstalk mechanisms to exacerbate tumor growth.

In the crosstalk between tumor cell EVs and the bone microenvironment, osteoblasts seem to play a crucial role, integrating the messages from cancer cell EVs. In fact, osteoblast preconditioning with breast cancer cell–derived factors resulted in their EVs gaining enhanced osteoclastogenic potential, indicating that the breast cancer secretome could enhance osteoblast EV–mediated osteoclastogenesis. We hypothesized that the enhanced osteoclastogenesis could be due to the enrichment of RANKL on the OB-EV surface, as demonstrated by cytofluorometry. This is consistent with several reports that suggest the implication of RANKL in cancer-mediated osteolysis,[6] and with our previous work demonstrating a dampened osteoclastogenic potential in *Tnfsf11*(*Rankl*)$^{-/-}$ OB-EVs.[13] The fact that supplementation of a suboptimal concentration of RANKL is needed to induce the formation of mature osteoclasts does not subtract from the results because the number of TRAcP-positive mononuclear cells was increased even without RANKL supplementation. However, in a microenvironment such the metastatic one, many other osteoclastogenic regulators can be enhanced (ie, soluble RANKL, Il6, CXCL2) or reduced (ie, OPG).

On the angiogenesis side, OB-EVs enhanced in vitro tube formation and in vivo angiogenesis in plug assay experiments, following pretreatment with breast cancer cell–derived factors, even more than MDA-EVs alone. We therefore speculate that breast cancer–derived factors reprogram osteoblasts to generate a premetastatic niche, conferring both osteolytic and angiogenic potential through educated OB-EVs and soluble factors. These findings collectively demonstrate the ability of metastatic breast cancer cell–derived EVs to establish a pro-osteoclastogenic and pro-angiogenic microenvironment through the regulation of the osteoblast secretome.

Intriguingly, MCF7, a very low metastatic, ER-positive breast cancer cell line, only partially reproduced the MDA-EVs mediated effects. In fact, although osteoblast gene expression was similarly affected, MCF7 did not influence osteoblast number. Furthermore, MCF7-EVs did not cause any pro-osteoclastogenic effect and, when OB-EVs were pre-educated with MCF7 CM, they failed to induce osteoclastogenesis even with suboptimal RANKL supplementation. In contrast, MCF7-EVs did show the ability to influence in vitro angiogenesis.

Finally, our *in vivo* analyses showed that MDA-EVs were recruited by the bone microenvironment and targeted osteoclasts, osteoblasts, and a few BM cells.

In conclusion, we have profiled and evaluated the effects of osteoblast-derived and breast cancer–derived EVs on the bone microenvironment in the context of the metastatic breast cancer. As summarized in Fig. 9, we found that both secreted factors and EVs from breast cancer cells are able to condition the bone microenvironment toward an osteolytic and angiogenic phenotype, and that this occurs at least in part through the influence of the osteoblast secretome and through the alteration of the biology of their EVs. Our findings therefore collectively show a previously undescribed role for breast cancer cell–derived EVs to condition and prime the bone microenvironment for metastasis.

Disclosures

The authors have no conflicts to disclose.

Acknowledgments

This work was supported by grants from the "Associazione Italiana per la Ricerca sul Cancro" (AIRC, #IG2015Id.16826) to NR and from the "Ricerca Finalizzata #RF-20130235739 to AT and MM. We are indebted to Dr Rita di Massimo for her contribution in editing this manuscript. We also thank Maria Giammatteo and Lorenzo Arrizza for their precious support with microscopy analyses.

Authors' roles: Study design: AT, MM, AC, and NR. Study conduct: AL, CG, AU, KS, AG, RP, MP, SDM, and NR. Data collection: AL, AC, CG, AU, KS, AG, RP, MP, SDM, and NR. Data analysis: AL, AC, CG, AU, KS, AG, RP, MP, SDM, and NR. Data interpretation: AL, AC, SDM, MM, AT, and NR. Manuscript drafting: AL and NR. Manuscript revision: AL, AC, MM, AT, and NR. Approving of final manuscript: AL, AC, CG, AU, KS, AG, RP, MP, SDM, MM, AT, and NR.

References

1. Coleman RE, Rubens RD. The clinical course of bone metastases from breast cancer. Br J Cancer. 1987;55:61–6.
2. Coleman RE, Smith P, Rubens RD. Clinical course and prognostic factors following bone recurrence from breast cancer. Br J Cancer. 1998; 77:336–40.
3. Lacey DL, Timms E, Tan HL, et al. Osteoprotegerin ligand is a cytokine that regulates osteoclast differentiation and activation. Cell. 1998;93: 165–76.
4. Yasuda HY, Shima N, Nakagawa N, et al. Osteoclast differentiation factor is a ligand for osteoprotegerin/osteoclastogenesis-inhibitory factor and is identical to TRANCE/RANKL. Proc Natl Acad Sci U S A. 1998;95:3597–602.
5. Cappariello A, Maurizi A, Veeriah V, Teti A. The Great Beauty of the osteoclast. Arch Biochem Biophys. 2014;558:70–8.
6. Maurizi A, Rucci N. The osteoclast in bone metastasis: player and target. Cancers (Basel). 2018;10(7):218.
7. Cox TR, Rumney RMH, Schoof EM, et al. The hypoxic cancer secretome induces pre-metastatic bone lesions through lysyl oxidase. Nature. 2015;522:106–10.
8. Becker A, Thakur BK, Weiss JM, Kim HS, Peinado H, Lyden D. Extracellular vesicles in cancer: cell-to-cell mediators of metastasis. Cancer Cell. 2016;30:836–48.
9. Valadi H, Ekström K, Bossios A, Sjöstrand M, Lee JJ, Lötvall JO. Exosome-mediated transfer of mRNAs and microRNAs is a novel mechanism of genetic exchange between cells. Nat Cell Biol. 2007;9:654–9.
10. Gangoda L, Liem M, Ang CS, et al. Proteomic profiling of exosomes secreted by breast cancer cells with varying metastatic potential. Proteomics. 2017;17:1–5.
11. Hashimoto K, Ochi H, Sunamura S, et al. Cancer-secreted hsa-miR-940 induces an osteoblastic phenotype in the bone metastatic microenvironment via targeting ARHGAP1 and FAM134A. Proc Natl Acad Sci U S A. 2018;115:2204–9.
12. Tiedemann K, Sadvakassova G, Mikolajewicz N, et al. Exosomal release of L-plastin by breast cancer cells facilitates metastatic bone osteolysis. Transl Oncol. 2019;12:462–74.
13. Cappariello A, Loftus A, Muraca M, Maurizi A, Rucci N, Teti A. Osteoblast-derived extracellular vesicles are biological tools for the delivery of active molecules to bone. J Bone Miner Res. 2018;33:517–33.
14. Marzia M, Sims NA, Voit S, et al. Decreased c-Src expression enhances osteoblast differentiation and bone formation. J Cell Biol. 2000;151: 311–20.
15. Rucci N, Rufo A, Alamanou M, et al. The glycosaminoglycan-binding domain of PRELP acts as a cell type-specific NF-kappaB inhibitor that impairs osteoclastogenesis. J Cell Biol. 2009;187:669–83.
16. Kruger S, Abd-Elmageed ZY, Hawke DH, et al. Molecular characterization of exosome-like vesicles from breast cancer cells. BMC Cancer. 2014;14:44.
17. Kubota Y, Kleinman HK, Martin GR, Lawley TJ. Role of laminin and basement membrane in the morphological differentiation of human endothelial cells into capillary-like structures. J Cell Biol. 1995;107: 1589–98.
18. Peramuhendige P, Marino S, Bishop RT, et al. TRAF2 in osteotropic breast cancer cells enhances skeletal tumor growth and promotes osteolysis. Sci Rep. 2018;8:39.
19. Rucci N, Capulli M, Piperni SG, et al. Lipocalin 2: a new mechanoresponding gene regulating bone homeostasis. J Bone Miner Res. 2015;30:357–68.
20. Ören B, Urosevic J, Mertens C, et al. Tumor stroma-derived lipocalin-2 promotes breast cancer metastasis. J Pathol. 2016;239:274–85.
21. Théry C, Amigorena S, Raposo G, Clayton A. Isolation and characterization of exosomes from cell culture supernatants and biological fluids. Curr Protoc Cell Biol. 2006;Chapter 3:22.1–29.
22. Lin HY, Sun SM, Lu XF, et al. CCR10 activation stimulates the invasion and migration of breast cancer cells through the ERK1/2/MMP-7 pathway. Int Immunopharmacol. 2017;51:124–30.
23. Oba Y, Lee JW, Ehrlich LA, et al. MIP-1alpha utilizes both CCR1 and CCR5 to induce osteoclast formation and increase adhesion of myeloma cells to marrow stromal cells. Exp Hematol. 2005;33:272–8.
24. Sabokbar A, Mahoney DJ, Hemingway F, Athanasou NA. Non-canonical (RANKL-independent) pathways of osteoclast differentiation and their role in musculoskeletal diseases. Clin Rev Allergy Immunol. 2016;51:16–26.
25. Xuan W, Feng X, Qian C, et al. Osteoclast differentiation gene expression profiling reveals chemokine CCL4 mediates RANKL-induced osteoclast migration and invasion via PI3K pathway. Cell Biochem Funct. 2017;35:171–7.
26. Li DQ, Wan QL, Pathak JL, Li ZB. Platelet-derived growth factor BB enhances osteoclast formation and osteoclast precursor cell chemotaxis. J Bone Miner Metab. 2017;35:355–65.
27. Vallet S, Pozzi S, Patel K, et al. A novel role for CCL3 (MIP-1α) in myeloma-induced bone disease via osteocalcin downregulation and inhibition of osteoblast function. Leukemia. 2011;25:1174–81.
28. Kubota K, Sakikawa C, Katsumata M, Nakamura T, Wakabayashi K. Platelet-derived growth factor BB secreted from osteoclasts acts as an osteoblastogenesis inhibitor factor. J Bone Miner Res. 2002;17:257–65.
29. Tawara K, Bolin C, Kancisky J, et al. OSM potentiates preintravasation events, increases CTC counts, and promotes breast cancer metastasis to the lung. Breast Cancer Res. 2018;20:53.
30. Bolin C, Tawara K, Sutherland C, et al. Oncostatin M promotes mammary tumor metastasis to bone and osteolyitic bone degradation. Genes Cancer. 2012;3:117–30.
31. Roberti MP, Arriaga JM, Bianchini M, et al. Protein expression changes during human triple negative breast cancer cell line progression to lymph node metastasis in a xenografted model in nude mice. Cancer Biol Ther. 2012;13:1123–40.
32. Palacios-Arreola MI, Nava-Castro KE, Castro JI, García-Zepeda E, Carrero JC, Morales-Montor J. The role of chemokines in breast cancer pathology and its possible use as therapeutic targets. J Immunol Res. 2014;2014:849720.
33. Strieter RM, Burdick MD, Mestas J, Gomperts B, Keane MP, Belperio JA. Cancer CXC chemokine networks and tumor angiogenesis. Eur J Cancer. 2006;42:768–78.
34. Ben-Baruch A. The multifaceted roles of chemokines in malignancy. Cancer Metastasis Rev. 2006;25:357–71.
35. Hardaway AL, Herroon MK, Rajagurubandara E, Podgorski I. Marrow adipocyte-derived CXCL1 and CXCL2 contribute to osteolysis in metastatic prostate cancer. Clin Exp Metastasis. 2015;32:353–68.
36. Davies SR, Watkins G, Mansel RE, Jiang WG. Differential expression and prognostic implications of the CCN family members WISP-1, WISP-2 and WISP-3 in human breast cancer. Ann Surg Oncol. 2007; 14:1909–18.
37. Johansson ME, Hansson GC. Microbiology. Keeping bacteria at a distance. Science. 2011;334:182–3.
38. Li Q, Wang H, Zogopoulos G, et al. Reg proteins promote acinar-to-ductal metaplasia and act as novel diagnostic and prognostic markers in pancreatic ductal adenocarcinoma. Oncotarget. 2016;7:77838–53.
39. Kaplan RN, Rafii S, Lyden D. Preparing the "soil": the premetastatic niche. Cancer Res. 2006;66:11089–93.
40. Peinado H, Zhang H, Matei IR, et al. Pre-metastatic niches: organ-specific homes for metastases. Nat Rev Cancer. 2017;17:302–17.
41. De Benedetti F, Rucci N, Del Fattore A, et al. Impaired skeletal development in interleukin-6-transgenic mice: a model for the impact of

chronic inflammation on the growing skeletal system. Arthritis Rheum. 2006;54:3551–63.

42. Peruzzi B, Cappariello A, del Fattore A, Rucci N, de Benedetti F, Teti A. C-Src and IL-6 inhibit osteoblast differentiation and integrate IGFBP5 signalling. Nat Commun. 2012;3:630.

43. del Fattore A, Cappariello A, Capulli M, et al. An experimental therapy to improve skeletal growth and prevent bone loss in a mouse model overexpressing IL-6. Osteoporos Int. 2014;25:681–92.

44. Capulli M, Ponzetti M, Maurizi A, et al. A complex role for Lipocalin 2 in bone metabolism: global ablation in mice induces osteopenia caused by an altered energy metabolism. J Bone Miner Res. 2018; 33:1141–53.

45. Mao L, Li X, Gong S, et al. Serum exosomes contain ECRG4 mRNA that suppresses tumor growth via inhibition of genes involved in inflammation, cell proliferation, and angiogenesis. Cancer Gene Ther. 2018; 25:248–59.